ACS APPLIED MATERIALS & INTERFACES

Research Article

www.acsami.org

Scalable Fabrication of High-Performance NO_2 Gas Sensors Based on Tungsten Oxide Nanowires by On-Chip Growth and RuO_2-Functionalization

Phung Thi Hong Van, Nguyen Hoang Thanh, Vu Van Quang, Nguyen Van Duy, Nguyen Duc Hoa, and Nguyen Van Hieu*

International Training Institute for Materials Science (ITIMS), Hanoi University of Science and Technology (HUST), Dai Co Viet Road, Hanoi, Vietnam

Supporting Information

ABSTRACT: The on-chip growth and surface-functionalization have been recently regarded as promising techniques for large-scale fabrication of high performance nanowires gas sensors. Here we demonstrate a good NO_2 gas-sensing performance of the tungsten oxide nanowires (TONWs) sensors realized by scalable on-chip fabrication and RuO_2-functionalization. The gas response (R_g/R_a) of the RuO_2-functionalized TONWs to 5 ppm of NO_2 was 186.1 at 250 °C, which increased up to ~18.6-fold compared with that of the bare TONWs. On the contrary, the responses of the bare and functionalized sensors to 10 ppm of NH_3, 10 ppm of H_2S and 10 ppm of CO gases were very low of about 1.5, indicating the good selectivity. In addition, the TONW sensors fabricated by the on-chip growth technique exhibited a good reversibility up to 7 cycles switching from air-to-gas with a response of 19.8 ± 0.033 (to 1 ppm of NO_2), and this value was almost the same (about 19.5 ± 0.027) for 11 cycles after three months storage in laboratory condition. The response and selectivity enhancement of RuO_2-functionalzied TONWs sensors was attributed to the variation of electron depletion layer due to the formation of RuO_2/TONWs Schottky junctions and/or the promotion of more adsorption sites for NO_2 gas molecule on the surface of TONWs, whereas the good reversibility was attributed to the formation of the stable monoclinic WO_3 from the single crystal of monoclinic $W_{18}O_{49}$ after annealing at 600 °C.

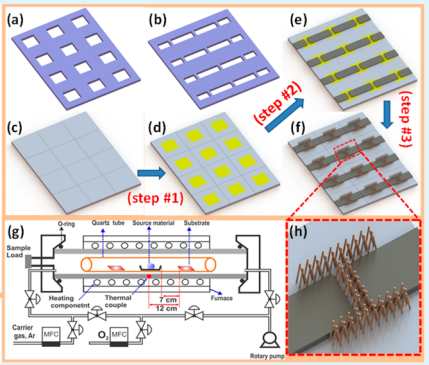

KEYWORDS: *tungsten oxide, nanowires, gas sensor, on-chip growth*

1. INTRODUCTION

Tungsten oxide, as an important semiconductor metal oxide, have a wide range of applications such as electrochromic devices, photocatalytic, field-emission displays, dye-sensitized solar cells, optical data storage, and gas sensors.[1] Numerous nanostructures of tungsten oxide have successfully synthesized make it a great candidate for gas sensors to detect highly toxic gases.[2] High performance gas sensors based on tungsten oxide nanostructures have been increasingly demonstrated.[3,4] Among nanostructured tungsten oxide, the nanowires (NWs) been received great attention for gas-sensing applications because of their unique properties.[5,6] For instant, TONWs-based gas sensors can be effectively functionalized by catalytic nanoparticles on the surface to enhance both the sensitivity and selectivity likely,[7] and they can be used to developed self-heating gas sensors working at ultralow power consumption.[8,9] With regard to the surface-functionalization, TONWs functionalized with Pd and Pt nanoparticles have been recently reported for enhanced sensitivity to H_2, CH_4 and C_2H_5OH gases.[10−12]

So far, TONWs for gas-sensing applications could be prepared through various methods including heat-treatment of tungsten foil,[13] thermal evaporation,[14] and wet-chemical approach.[15] Frequently, the gas sensors based on TONWs were fabricated via the postsynthesis technique, in which TONWs are synthesized, collected and then coated on prefabricated electrodes substrates.[3,4,10,11] As for the metal oxides NWs gas sensors, the NWs-NWs junctions play an important role on gas-sensing performance,[16] which could not form naturally on the electrodes by using the postprocess methods, and this could not result in as-expected gas-sensing response and stability of the NWs-based sensors.[17] The on-chip growth is one of the most promising fabrication platforms for NWs gas sensors, which has been investigated by some research groups[16,18−20] and present authors.[21,22] Most of the works demonstrated the on-chip fabrication technique have focused on SnO_2 and ZnO NWs, but not yet on TONWs. Our recent works reported about TONWs-based gas sensors[23,24] were also not yet applied by the on-chip fabrication technique. In the present work, we have developed an effective process for on-chip fabrication of TONWs via thermal evaporation methods using W film as seeds layer. As-obtained sensors were measured with NO_2 gas and different operating temperatures. Subsequently, to enhance

Received: February 20, 2014
Accepted: July 1, 2014
Published: July 1, 2014

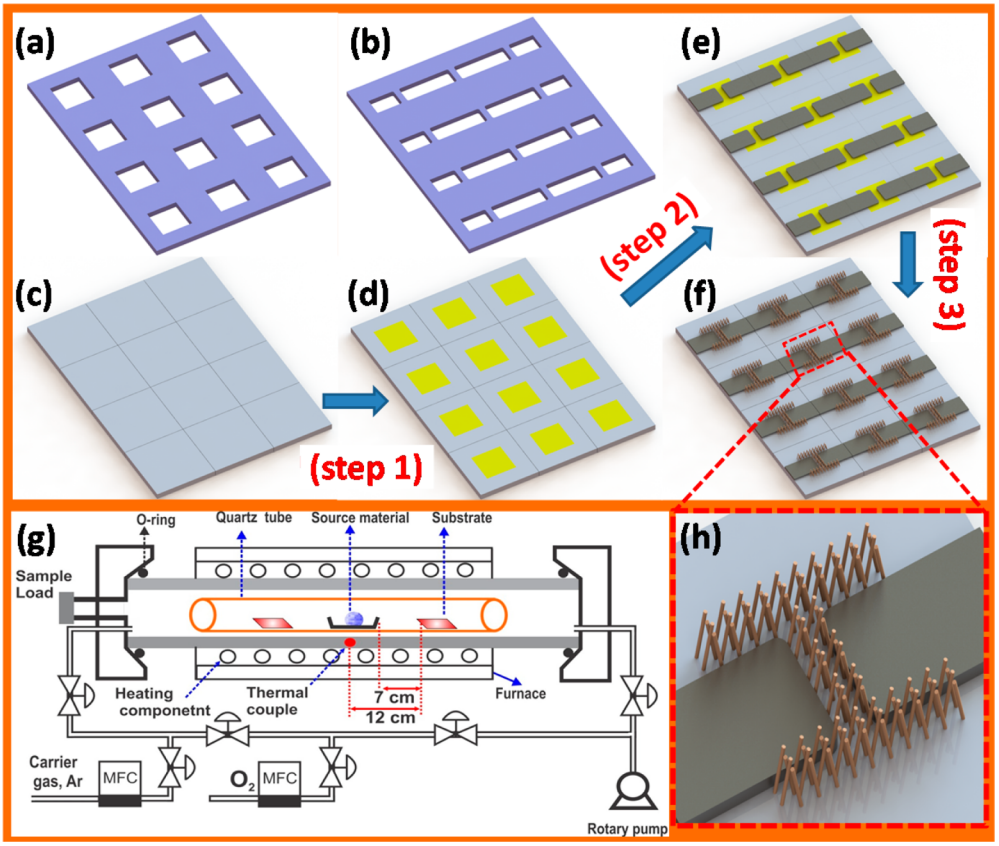

Figure 1. On-chip fabrication process of TONWs included: (step 1) sputtering 30 nm W through first metal shadow mask (a) on Al_2O_3 substrate (c) to form as catalyst layer (d); (step 2) sputtering Pt through second metal shadow mask (b) to form two pillar electrodes (e); and (step 3) the growth of TONWs (f, h) using a thermal evaporation setup (g).

the sensitivity and selectivity to NO_2 gas, the TONWs sensors were functionalized with RuO_2 nanoparticles. In the on-chip fabrication process, TONWs were integrated into electrodes in a single-step way, so it can minimize the surface contamination because of the electrode posts' prefabrication. These NWs sensors were effectively functionalized with RuO_2 for significantly enhancing NO_2 gas-sensing performance. This method could be used for scalable fabrication of TONWs sensors with relatively high yield. As-developed sensors can be a potential candidate for various applications such as air-quality monitoring (a need of detection of NO_2 gas concentrations from few ppb to ppm), monitoring air pollution of hazardous environment (a need of gas sensors with good stability) and car emission control.

2. EXPERIMETAL SECTION

The fabrication procedures for on-chip fabrication of TONWs gas sensors are shown in Figure 1. An Al_2O_3 substrate (size 20 mm × 15 mm; thickness 0.25 mm) was scribed by laser to separate into 12 chips (size 5 mm × 5 mm) as shown in Figure 1c. The substrate were ultrasonically cleaned with acetone and ethanol for 20 min each followed by blow drying with nitrogen gas. In step 1, the square-shaped W seed layers (thickness: ∼20 nm) were deposited by sputtering through the first shadow metal mask (Figure 1a). In step 3, the pillar-shaped Pt electrodes (thickness 200 nm) were also deposited by sputtering through the second shadow metal mask (Figure 1b). As-obtained substrate contains 12 pairs of Pt electrodes (i.e., 12 sensor chips) with a gap of ∼1 mm (Figures 1e). In step 3, the TONWs were then grown on the substrate via thermal evaporation of WO_3 powder source using thermal evaporation setup as previously described.[23] The Al_2O_3 boat (size the length of ∼10 cm and the width of ∼1 cm) filled with about 0.3 g of WO_3 powder (99.98%, BDH Chemicals Poole England) and the substrate with 12 sensor chips were loaded in the middle of a quartz tube (size length of 60 cm and inner diameter of 2.5 cm) as shown in Figure 1g. The TONW is expected selective growth on the predeposited tungsten layers as described in Figure 1h. Note that the distance between the boat and the substrate was placed far away from the boat ∼7 cm. Then the completed quartz tube was placed in the horizontal tube furnace of the thermal evaporation so that the boat located in the center of the furnace [the position of thermal couple, Figure 1g]. After evacuation to $\sim 10^{-2}$ Torr by using a rotary pump, the reacted quartz tube was filled with Ar gas (99.99%) to atmosphere pressure and pumped down again to 10^{-2} Torr (this step was repeated about 4 or 5 times). After that the furnace was heated up to 1000 °C in 1 h, and held in 2 h for the NWs growth, followed by cooling down to room temperature in 4 h to get the sensor chips. No carrier gas was introduced into the reaction tube. The pressure increase was caused by the leakage of air into and outgassing from vacuum components. Hence, the pressure inside the tube was estimated to be ∼4 Torr. The decorating TONWs with RuO_2 nanoparticles was performed through the deposition of a solution containing the Ru-precursor [$Ru(COOCH_3)_2$] using a micropipette (10 μL), followed by a heat-treatment at 600 °C. Different concentrations (1, 10, and 100 mM) of the Ru-precursor solution were used to control the density of RuO_2 on the NWs surface in this investigation. The morphologies of the TONWs were characterized by field emission scanning electron microscopy (FE-SEM, Hitachi S-4800, Japan), high resolution transmission electron microscopy (HRTEM, JEM-3010 HR by JEOL), and an X-ray diffraction (XRD, Philips Xpert Pro) with a CuKα (wavelength: 0.15418 nm) radiation source operated at a voltage of 40 kV.

Operational principle of sensors based on the variation in electrical resistance of devices upon exposure to analytic gas. Therefore, to evaluate the gas-sensing characteristics of the sensors, the resistance of

the devices was continuously measured upon time, and the environmental ambient gas was switched on/off from air to target gas.[23] Measurements of the gas-sensing characteristics were performed by using flow-through technique with a standard flow rate of 200 sccm (standard cubic centimeters per minute) for both reference (dry air) and target gases, at different temperatures (200, 250, and 300 °C), and to NO_2 gas (1−5 ppm) other gases such as NH_3 (10 ppm), H_2S (10 ppm), and CO (10 ppm). The gas sensor was mounted on a hot-plate and equipped with two tungsten needles as 2 DC-probes, and the gas-line was directly exposed to the surface of WO_3 NWs sensors. Configuration of the gas-sensing chamber can be seen in Figure S1 (Supporting Information). Details about the experimental setup for measuring the gas-sensing characteristics of the sensors were reported in our previous work.[25] The resistance of the sensors was measured by two-point configuration using a voltage source meter (Keithley 2602) interfaced with a computer.

3. RESULTS AND DISSCUSION

An optical image of as-sputtered Pt pillar electrodes and as-fabricated TONWs is shown in Figure 2a and b, respectively.

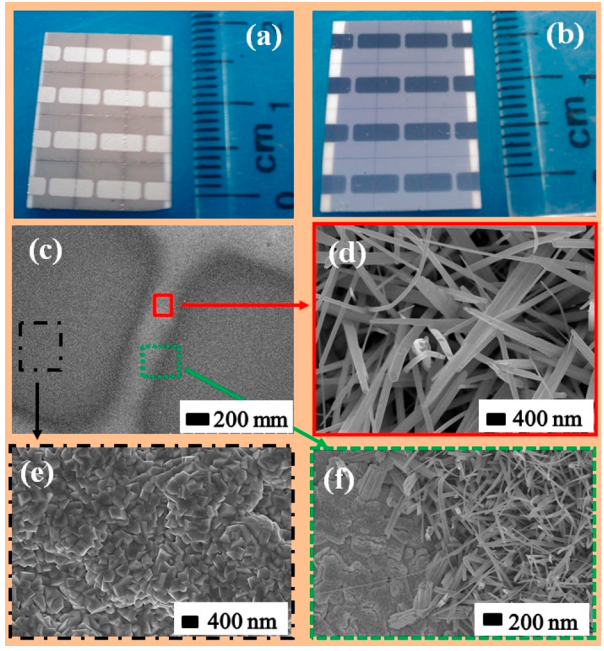

Figure 2. As-obtained TONWs sensors: (a) Al_2O_3 substrates with presputtering W layer and Pt electrodes; (b) the TONWs grown on the Al_2O_3 substrates; (c) low magnification SEM image of the TONWs sensors, higher magnification SEM image focused on area between electrodes (d), Pt electrode (e), and the border between Pt electrode and NWs (f).

There are 12 sensor chips were fabricated in one run of thermal evaporation process. The TONWs were uniformly grown on the Al_2O_3 substrate, this demonstrates that this route can be used to realize TONWs gas sensor on a large scale. The surface of as-fabricated sensor chips were characterized at selected positions by FE-SEM and the results are shown in Figure 2c−f. As can be seen TONWs selectively grown on the area of W seed layer but neither on Pt electrode nor Al_2O_3 bare substrate (Figure 2e and f). As-grown TONWs show a highly porous structure, and a network NWs is also formed for electron conduction between the two Pt electrodes (Figure 2d). The high magnification FE-SEM image shows that tungsten NWs are several tens of micrometers long and 90−300 nm diameter. Compared with previous work,[23] in which TONWs grown on W substrate covered on the boat, the morphology of the TONWs from present work is relatively different. This is attributed to the use of W layer as seed and the placement at lower temperature region (the temperature of substrate region is around 880 °C).

The detail microstructures of as-synthesized TONWs were characterized by using TEM. Typical TEM image of a TONW is shown in Figure 3a. The surface of TONWs is quite smooth

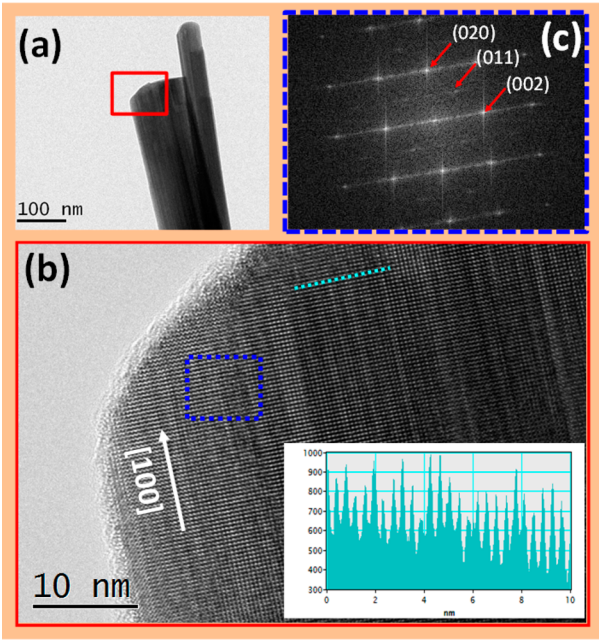

Figure 3. TEM mage of TONWs (a), selected diffraction area (b), HRTEM image of the NWs and element mapping on a distance of 10 nm corresponding to 26 planes (c).

and its diameter is around ∼100 nm. The HRTEM image and corresponding fast Fourier transformation (FFT) of the same TONW are shown in Figure 3b and 3c, respectively. They indicate that the TONWs is single crystalline with preferred growth direction of [100]. The inset in Figure 3b is the scanning of 10 nm in length along the same TONW, indicating about 26 planes. This means the lattice fringes of TONW are around 0.38 nm, which is indexed to be the (010) plane of monoclinic $W_{18}O_{49}$.

The XRD characterizations of as-grown TONWs and after annealing at 600 °C are shown in Figure 4. The diffraction peaks of as-synthesized TONWs (Figure 4a) can be well indexed to monoclinic $W_{18}O_{49}$ phase with unit cell parameters of a = 18.32 Å, b = 3.784 Å, c = 14.03 Å, and β = 115.20 (JCPDS: 36−0101). In the XRD patterns, the (010) diffraction peak was the strongest. This result indicates that the [010] is the dominant growth direction of the NWs that agreed with TEM characterization. The diffraction peaks of TONWs after annealing at 600 °C (Figure 4b) the diffraction peaks can be well indexed to monoclinic WO_3 phase with unit cell parameters of a = 7.297 Å, b = 7.539 Å, c = 7.688 Å, and β = 90.91 (JCPDS 43-1035). These parameters are consistent with those reported in previous works.[26,27]

The growth mechanism of TONWs from the present work is similar to previous works.[14,23] Both W seed layer and WO_3 powder source are crucial to ensure the successful growth of TONWs. To verify this, we have conducted two other

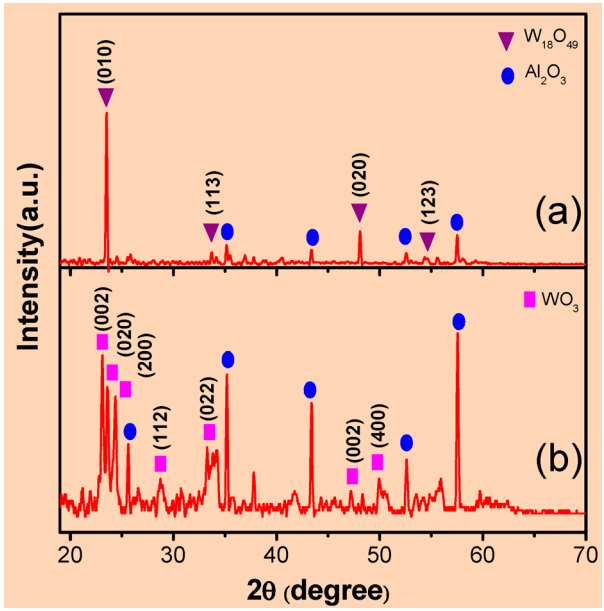

Figure 4. XRD patterns of the as-obtained NWs after growth (a) and annealing at 600 °C (b).

experiments without using W seed layer (i.e., the use of bare Al_2O_3 substrate) or WO_3 powder source (i.e., the use of empty Al_2O_3 boat) with keeping other growth parameters, and TONWs were not observed from the both experiments (data not show). The results revealed that the TONWs were not observed on the substrate when the WO_3 powder source or the W seed layer was not used. This is to rule out the possibility of TONWs grown directly from the oxidation of the W layer as previous report[28] and to convince the necessary of W seed layer for TONWs growth as previous work.[29] We also grew TONWs with the use of W seed layer with different thickness (10, 20, 30 nm), the as-obtained TONWs were very similar. Although the seed layer is needed for TONWs growth, the growth mechanism is unlikely to be the typical vapor−liquid−solid (VLS) mechanism. This is because seed nanoparticles were not found at the top or bottom of TONWs as similar as the NWs grown by VLS mechanism. So the growth mechanism of TONWs from the present work seems to be VS mechanism as previous reports.[23,29−32] The role of the W seed layer oxidized by heating under the growth pressure is provided nucleation site for TONWs growth, and it is promoted by modifying the adsorption and diffusion characteristics of the substrate surface to be become a preferential place for adsorbing and trapping of tungsten oxide vapor.[31,32] This suggests that the W seed layer should be used for selected growth of TONWs.

Before gas-sensing measurements, the as-obtained TONWs sensor was annealed at 600 °C for 5 h to stabilize the resistance of the sensors. The gas-sensing response was statically measured on 12 sensors at the same substrate (Figure 5a), and their resistance transient responses to 1 ppm of NO_2 and at 300 °C are shown in Figure 5b. Because the prototype sensors did not content the microheater, thus external heater was used to heat up the sensor to operating temperate. However, to use these sensors in real environment, the compacted devices which included the heater, temperate sensors and back side etched to reduce the power consumption are all under developed in our laboratory using silicon technology and will be reported elsewhere. It can be seen that resistance in air and NO_2 gas seems to be in relatively large variation. The resistance in air (R_a) is in the range from 106 to 439 kΩ. The sensor response calculated by the ratio of R_g/R_a (R_g is the resistance in gas) is plotted corresponding to the position of the sensor chips on the substrate as shown in Figure 5c [rows 1, 2, 3, and 4 and columns B, C, and D]. It can be seen that the sensor response is varied in a relatively large range from 1.4 to 3.1. The gas sensing characteristics of random sensors obtained from four different fabrication runs were also checked to 1 ppm of NO_2 at temperature of 300 °C to evaluate the reproducibility of the synthesis process. The variation in response of different sensors was negligible (see Figure S2, Supporting Information), indicating the good reproducibility of the devices.

We believe that such large variations in the response and the resistance of the as-fabricated TONWs sensors can be improved by using a larger tubular thermal evaporation setup and a smaller chip-size for large-scale fabrication. Furthermore, using our synthesis method, it can be scalable fabrication of sensor chips by silicon microelectronic technology for improved cost efficiency of the process. The stability of gas sensors are one of the most important parameters influenced their reusability that should be taken into account for real-life application. To verify the stability of the gas response of the on-chip fabrication sensors, we recorded the sensor response by cycling between reference air and target gas (1 ppm of NO_2) at 300 °C for 7 times (7 cycles) and 11 times (11 cycles) on 3 months later, as shown in Figure 5d. The TONWs gas sensor exhibited very stable signals for 7 cycles of NO_2 gas and air exposure, and after 3 months, such stability was also observed for another 11 cycles. A statically analysis of the gas response before and after 3 months was showed in Figure 5(e). Very reproducible response with average variation of ∼1.7% (0.033/1.98) for the 7 cycles was observed. After 3 months, comparatively, the variation was about ∼1.4% (0.027/1.95) for 11 cycles. This result might be attributed to the highly crystalline structure of TONWs and natural formation of the network NWs on the substrate by using on-chip fabrication technique. The highly crystalline structure can diminish the grain growth and degradation under long-term operation at elevated temperatures and electrical transport as reported in previous work.[33] The NW-NW junctions play important role for gas-sensing performance of the network NWs sensors, and the supposed in situ formation of these junctions during growing NWs are more stable than that of postprocess.

A typical TONWs gas sensor was measured to 1, 2.5, and 5 ppm of NO_2 gas at 200, 250, and 300 °C. The transient resistances and the sensor response as a function of gas concentration are shown in Figure 6a−c and d, respectively. The sensor showed stable sensing and recovery characteristics regardless of the measured temperatures. The sensor responses to 1−5 ppm at temperature of 250 °C are in the range of from 2.7 to 10, which are higher than that at temperatures of 200 and 300 °C. The response value to 5 ppm of NO_2 was around 10.1 at 250 °C, which was decreased to 7.1 and 5.2 at 200 and 300 °C, respectively. Thus, the sensing-temperature of around 250 °C can be considered as an optimum operating temperature of the present TONWs sensors. This tendency is consistent with the variation of the NO_2 gas response of WO_3 NWs gas sensor in literature,[23,34] but such optimum operating temperature is higher than that of $W_{18}O_{49}$ NWs gas sensors as reported works.[4,35] Compared with recent works on the NO_2 gas sensors based on TONWs prepared by thermal evaporation and solvothermal methods,[29,35] the NO_2 gas-sensing response of

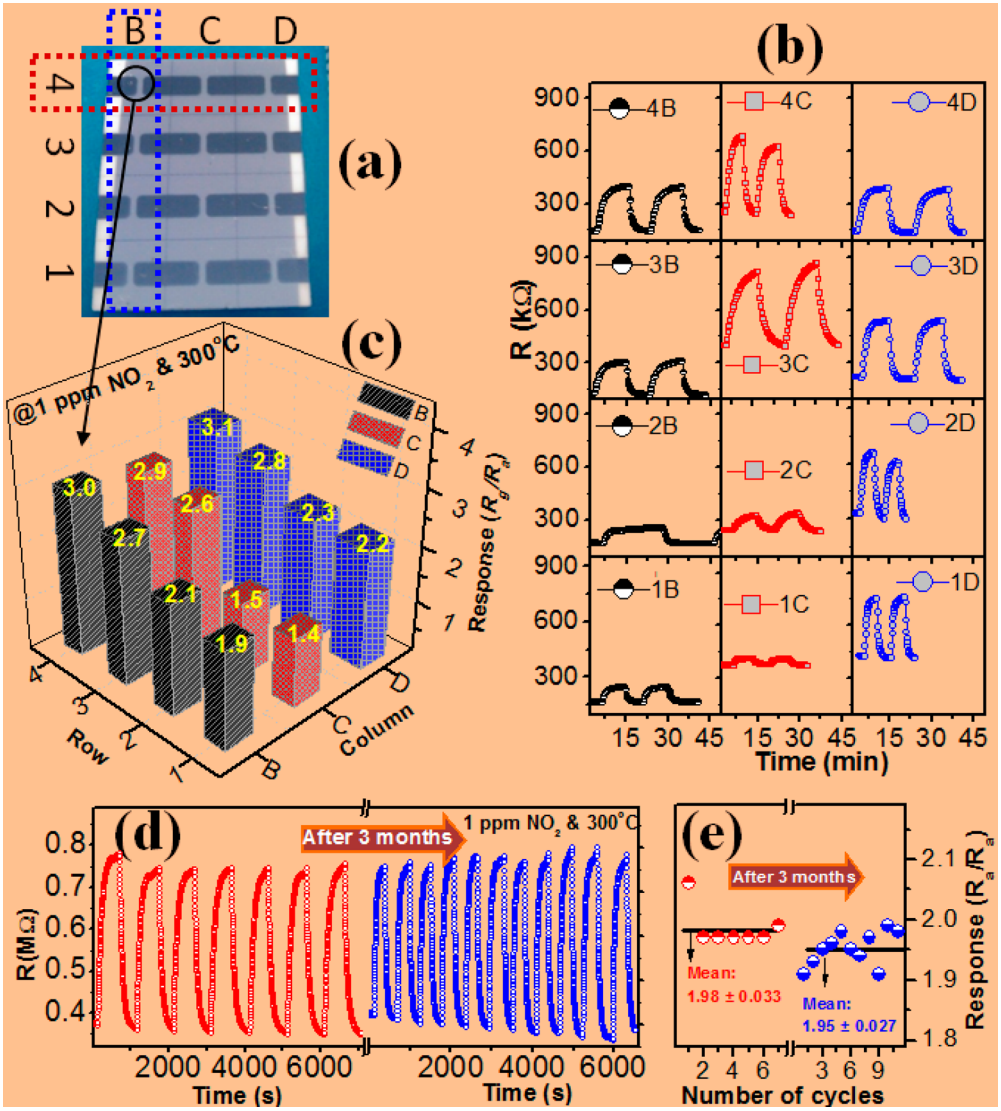

Figure 5. NO_2 sensing characteristics of 12 sensors obtained from one-run fabrication: (a) fabricated sensors on Al_2O_3 substrate, (b) dynamic sensing transients of the sensors measured at 1 ppm and 300 °C, (c) gas response distribution of the as-fabricated sensors on the chip, (d) dynamic sensing transient recorded by cycling between air and target gas for 7 times and another 11 times on 3 months later, and (e) statistics on gas response before and after 3 months.

the present work is relatively lower. However, the advantage of the present fabrication route is the cost-effective and facile method, which can employed to prepare highly crystalline TONWs network gas sensors on a large-scale. Such low responses to NO_2 gas can be attributed to following reasons: (i) a buffer layer always exits under the TONWs network film (i.e., making a leakage current between electrodes) and (ii) the average diameter of TONWs is relatively larger compared with that synthesized via thermal evaporation as reported in literature.[30,31] These issues can be improved by (i) designing novel structures for the on-chip growth of TONWs gas sensors such as air-bridged NWs-junctions sensors[36] and discrete island NWs-array network[37] and (ii) optimizing synthesized parameters to reduce the size of TONWs. Once the gas-sensing performance of TONWs sensors is improved, the scalable fabrication route of the present work can be absolutely employed for mass-production of TONWs gas sensors toward product commercialization. Because the present sensor fabrication protocol can be used to develop a large scale fabrication of TONWs sensors by employing large tube thermal evaporation system and designing sensor chip size in the range of μm. Despite that, for large scale production in industrial process, further study about the homogeneity and reproducibility are needed. To quickly demonstrate enhanced NO_2 gas-sensing response, we have carried out surface-functionalization of TONWs with the RuO_2, which has pronounced one of promised catalyst oxides for NO_2 gas sensors enhancement.[38] The FE-SEM images of bare TONWs and RuO_2-functionalized TONWs (RuO_2-TONWs) are shown in Figure 7a and b, respectively. Compared with bare TONWs, the surface of RuO_2-TONWs had distributive decoration of RuO_2 nanoparticles on their surface after heat-treating at 600 °C. To confirm this finding, the RuO_2-TONWs were examined by XRD and energy dispersive X-ray spectroscopy (EDX) as shown in Figure 7c and d, respectively. The XRD pattern of RuO_2-TONWs sample exhibited the coexistent phase of WO_3 and RuO_2 with their typical peaks identified from JCPDS Card No. 43-1035 and 40-1290. The EDX spectroscopy of the RuO_2-TONWs sample is composed not only W and O elements, but also Ru one. HRTEM image of the WO_3 nanowire decorated

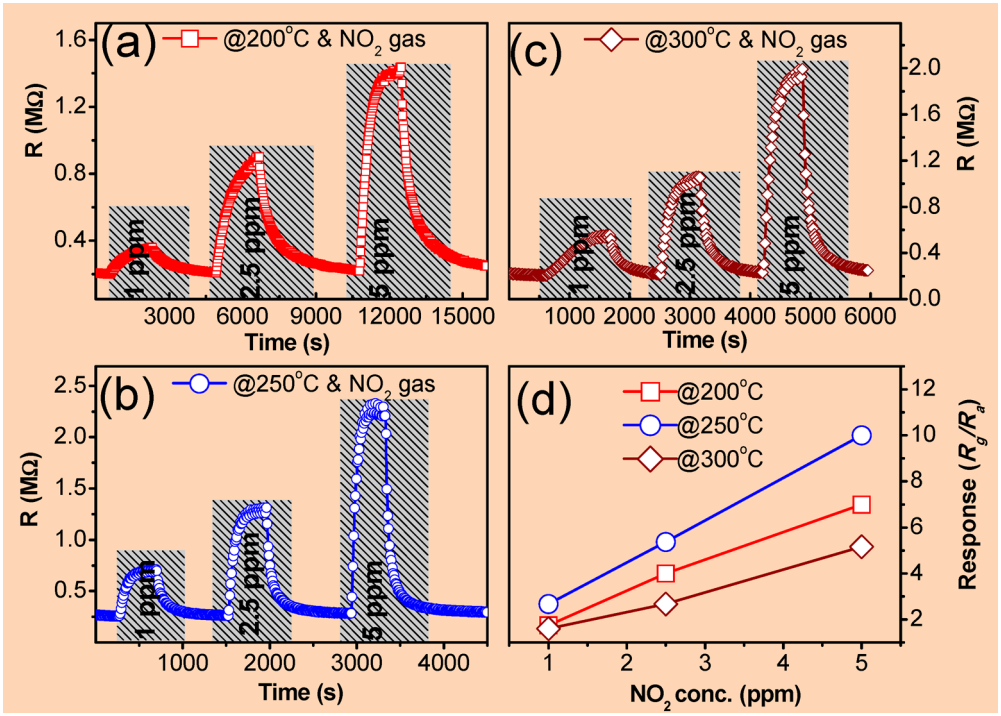

Figure 6. Dynamic NO_2 sensing transient of the TONWs sensors measured at 200 (a), 250 (b), and 300 °C (c). Gas response (R_g/R_a) plotted as a function of gas concentrations (d).

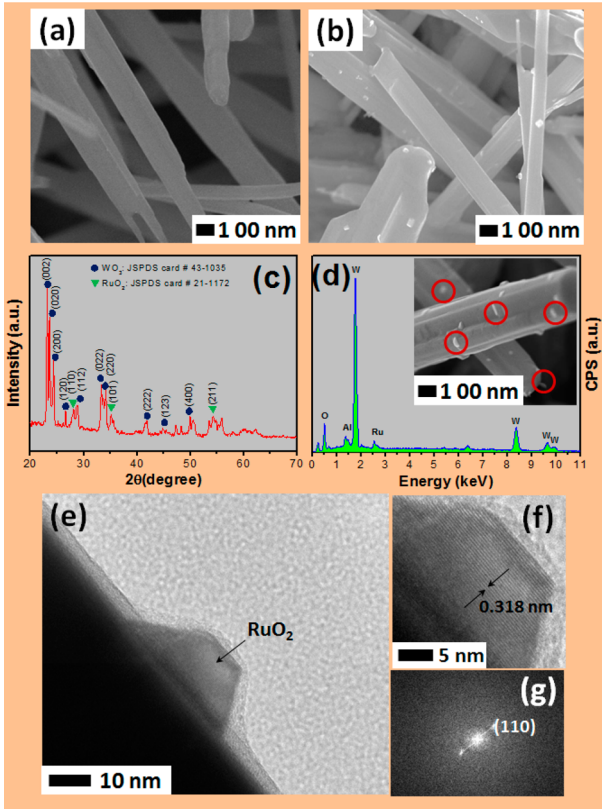

Figure 7. (a) FE-SEM images of TONWs, (b) FE-SEM images, (c) XRD pattern, and (d) EDS mapping of RuO_2-TONWs; (e, f) HRTEM images of RuO_2-TONWs (10 mM Ru-precursor sample), and corresponding fast Fourier transform (g) indicated that single crystal RuO_2 nanoparticle was effectively decorated on the surface of TONWs.

with RuO_2 nanoparticle is shown in Figure 7e. It is clearly that the RuO_2 nanoparticle with a size of about 10 nm decorates strongly on the surface of the WO_3 nanowire. The RuO_2 nanoparticle has a high crystallinity of a single crystal, as confirmed by a higher magnification HRTEM image (Figure 7f) and the corresponding fast Fourier transform (Figure 7g). The distance between lattice fringes calculated from the HRTEM image is about 0.318 nm, this value is consistent with the interspace of (110) planes of tetragonal RuO_2 (JCPDS, 40-1290; d_{110} = 0.318 nm). The fast Fourier transform also shows the two bright dots of (110) of single crystal RuO_2.[39]

RuO_2-TONWs sensor was then measured to 1, 2.5, and 5 ppm of NO_2 gas at 250 °C. Figure 8a–c showed the resistance transient of the RuO_2-TONWs gas sensors, in which the functionalization was conducted by using $Ru(COOCH_3)_2$ different solvents with concentration of 1, 10, and 100 mM. All the RuO_2-functionalized TONW gas sensors showed stable sensing and recovery characteristics at 250 °C. The NO_2 gas response as a function of the gas concentration is shown in Figure 8d, indicating that all the functionalized sensors have much better response to NO_2 gas compared to bare TONWs sensor.

The functionalized sensor using $Ru(COOCH_3)_2$ solvents with concentration of 10 mM relatively shows the most enhancement. The response to 1, 2.5, and 5 ppm of NO_2 gas is in the range from 14 to 188, which is higher than that compared with the bare TONW sensors. This suggests that the simple step of RuO_2 functionalization can result in a significantly enhanced NO_2 gas response. The gas response to 5 ppm of NO_2 at 250 °C of RuO_2-TONWs sensor is increased by a factor up to ~18.6-fold. The as-obtained responses to NO_2 gas of RuO_2-TONWs sensors are comparable with some of the highest responses reported in the literature for TONWs-based gas sensors.[3,29,35,40]

dx.doi.org/10.1021/am5010078 | ACS Appl. Mater. Interfaces 2014, 6, 12022–12030

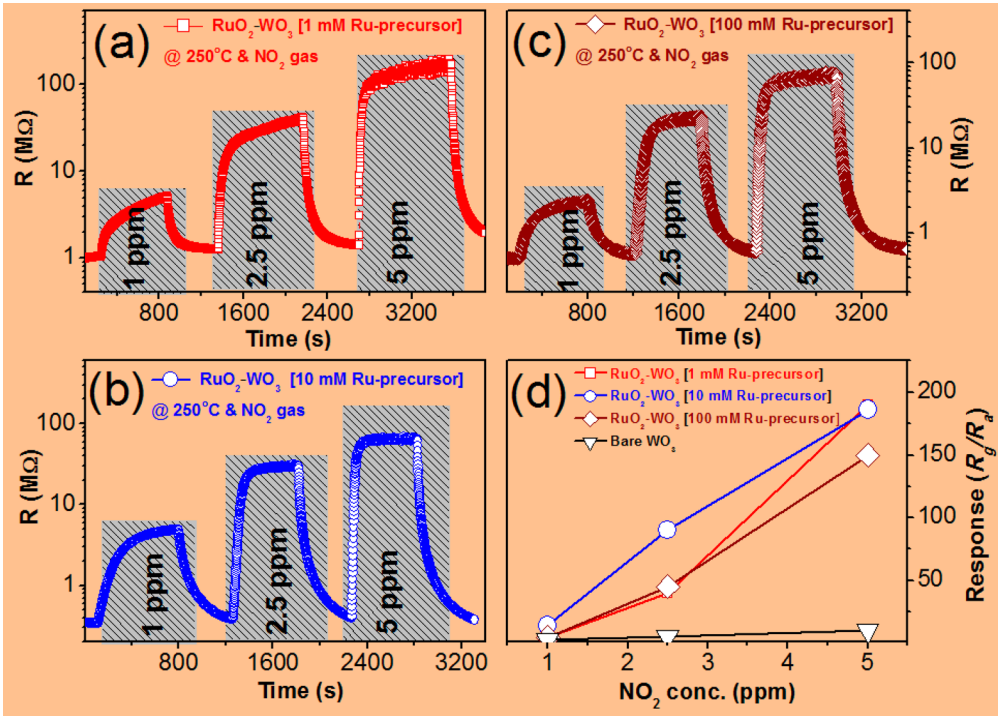

Figure 8. Dynamic NO_2 sensing transients of the WO_3 NWs sensors functionalized with RuO_2 using 1 (a), 10 (b), and 100 mM Ru-precursor solution (c). Gas response (R_g/R_a) plotted as a function of gas concentration (d).

The gas response of TONWs and RuO_2-TONWs sensors were individually measured with other gases such as NH_3, H_2S, and CO at 250 °C to investigate their selectivity, and the results are shown in Figure 9a. In the bare TONWs sensor, the gas

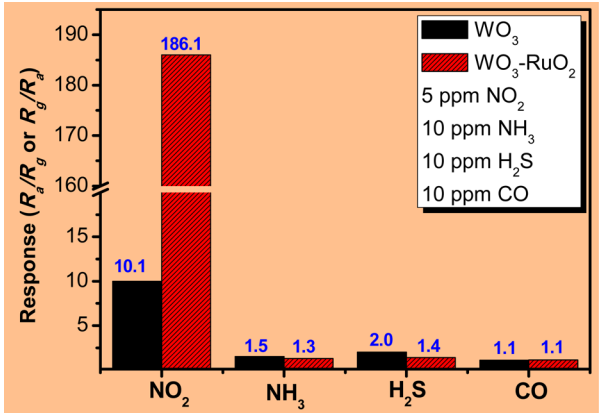

Figure 9. Gas response of bare WO_3 and RuO_2–WO_3 sensors to 5 ppm of NO_2 and 10 ppm of NH_3, H_2S, and CO.

response value to 5 ppm of NO_2 (R_g/R_a = 10.1) at 250 °C is not much higher than that to 10 ppm of NH_3 (R_a/R_g = 1.5), 10 ppm of H_2S (R_a/R_g = 2.1), and 10 ppm of CO (R_a/R_g = 1.1) (black bars, Figure 9a). Thus, the bare TONWs sensor seems to be difficult for selective detection of NO_2 gas in the present of NH_3, H_2S and CO gases. In contract, the RuO_2-TONWs sensor exhibited a great selectivity to NO_2 gas. The response value (R_g/R_a) to 5 ppm of NO_2 of this sensor at 250 °C was as high as 186, which is much higher than that to 10 ppm of NH_3 (R_a/R_g = 1.3), 10 ppm of H_2S (R_a/R_g = 1.4), and 10 ppm of CO (R_a/R_g = 1.2). The as-obtained selectivity to NO_2 gas of RuO_2-TONWs gas sensors from the present work are among the best achievement for NO_2 gas sensors based on various functionalized metal oxides NWs, such as Co_3O_4–ZnO NWs,[41] Pd-SnO_2 NWs,[42,43] and Pd–In_2O_3–NWs.[44] The developed RuO_2-TONWs sensors could detect highly toxic NO_2 gas at low concentration of less than 5 ppm, with good selectivity to NH_3, H_2S, and CO, thus they are suitable for application in monitoring of urban air pollution, petrol and metal refining, and manufacturing industries.

The enhanced the NO_2 gas response and the selectivity of RuO_2-TONWs can be attributed by two following mechanisms. First, the extension of the depletion layer at the neighborhood of RuO_2 nanoparticles (NPs) is due to the formation of Schottky junction of RuO_2/TONWs (RuO_2 is metallic characters[45]). This mechanism was frequently used to explain the enhanced gas-sensing performance of various NPs-functionalized NWs sensors in the literature.[10,12,46,47] Second, the RuO_2 NPs decorated on the surface of TONWs provide more active site for NO_2 adsorption because of their acting as catalyst site. The catalyst active of RuO_2 cannot explain based on the well know spillover effect as usual,[10,12,46,47] because this mechanism promotes more the adsorption of oxygen molecules (O_2^-, O^-, O^{2-}), resulting an enhanced gas response to reduced gases. We have found out that the catalyst active of RuO_2 can be explained based on "NO_2-traps" as reported.[48,49] The RuO_2 can be more efficiently trapped NO_2 and stored as nitrates (NO_3^-). However, we believe that further studies on the RuO_2-TONWs are needed to optimize and to understand the enhanced NO_2 gas-sensing performance. In additionally, the effect of humidity on the gas-sensing characteristics of the fabricated sensors was not systematically studied yet. However, during gas sensing measurement, dry air was used as reference and carrier gas using the flow-through technique thus we could ignore the effect of humidity.

4. CONCLUSION

In this work, we have fabricated single crystalline tungsten oxide nanowires sensors by the on-chip growth route using vapor phase reaction, which shows a facile and scalable fabrication method. The gas-sensing performance of the 12 sensor chips fabricated from one-run of thermal evaporation process was investigated. As-fabricated sensors showed relatively good response to NO_2 gas and good stability. The response and selectivity of the nanowires sensors to NO_2 gas exhibited a great improvement by simply functionalizing with RuO_2 nanoparticles. Both on-chip growth and surface-functionalization have great potential for development of novel nanowire gas sensors.

■ ASSOCIATED CONTENT

Supporting Information

Experimental setup used for gas-sensing characterizations of the present work and the transient response of the gas sensors obtained from different fabrication runs. This material is available free of charge via the Internet at http://pubs.acs.org/.

■ AUTHOR INFORMATION

Corresponding Author

*E-mail: hieu@itims.edu.vn/hieu.nguyenvan@hust.edu.vn. Phone: 84-4-38680787. Fax: 84-4-38692963.

Notes

The authors declare no competing financial interest.

■ ACKNOWLEDGMENTS

This research was funded by the Vietnam National Foundation for Science and Technology Development (Code 103.02-2014.18) and VLIR-UOS under the Research Initiative Project (ZEIN2012RIP20). Authors acknowledge to Dr. Nguyen Duc Dung at HUST and Laboratory of Geology, Geoengineering, Geoenvironment and Climate Change at Vietnam National University, Hanoi for HRTEM characterizations.

■ REFERENCES

(1) Zheng, H.; Ou, J. Z.; Strano, M. S.; Kaner, R. B.; Mitchell, A.; Kalantar-zadeh, K. Nanostructured Tungsten Oxide—Properties, Synthesis, and Applications. *Adv. Funct. Mater.* **2011**, *21*, 2175−2196.

(2) Chi, L.; Xu, N.; Deng, S.; Chen, J.; She, J. An Approach for Synthesizing Various Types of Tungsten Oxide Nanostructure. *Nanotechnology* **2006**, *17*, 5590−5595.

(3) Ponzoni, A.; Comini, E.; Sberveglieri, G.; Zhou, J.; Deng, S. Z.; Xu, N. S.; Ding, Y.; Wang, Z. L. Ultrasensitive and Highly Selective Gas Sensors Using Three-Dimensional Tungsten Oxide Nanowire Networks. *Appl. Phys. Lett.* **2006**, *88*, No. 203101.

(4) Zhao, Y. M.; Zhu, Y. Q. Room Temperature Ammonia Sensing Properties of $W_{18}O_{49}$ Nanowires. *Sens. Actuators B* **2009**, *137*, 27−31.

(5) Choi, K. J.; Jang, H. W. One-Dimensional Oxide Nanostructures as Gas-Sensing Materials: Review and Issues. *Sensors* **2010**, *10*, 4083−4099.

(6) Gurlo, A. Nanosensors: Towards Morphological Control of Gas Sensing Activity. SnO_2, In_2O_3, ZnO and WO_3 Case Studies. *Nanoscale* **2011**, *3*, 154−165.

(7) Kolmakov, A.; Chen, X.; Moskovits, M. Functionalizing Nanowires with Catalytic Nanoparticles for Gas Sensing Application. *J. Nanosci. Nanotechnol.* **2008**, *8*, 111−121.

(8) Prades, J. D.; Jimenez-Diaz, R.; Hernandez-Ramirez, F.; Barth, S.; Cirera, A.; Romano-Rodriguez, A.; Mathur, S.; Morante, J. R. Ultralow Power Consumption Gas Sensors Based on Self-Heated Individual Nanowires. *Appl. Phys. Lett.* **2008**, *93*, No. 123110.

(9) Zhu, L. F.; She, J. C.; Luo, J. Y.; Deng, S. Z.; Chen, J.; Ji, X. W.; Xu, N. S. Self-Heated Hydrogen Gas Sensors Based on Pt-Coated $W_{18}O_{49}$ Nanowire Networks with High Sensitivity, Good Selectivity and Low Power Consumption. *Sens. Actuators B* **2011**, *153*, 354−360.

(10) Chávez, F.; Pérez-Sánchez, G. F.; Goiz, O.; Zaca-Morán, P.; Peña-Sierra, R.; Morales-Acevedo, A.; Soledad-Priego, M. Sensing Performance of Palladium-Functionalized WO_3 Nanowires by a Drop-Casting Method. *Appl. Surf. Sci.* **2013**, *275*, 28−35.

(11) Kukkola, J.; Mohl, M.; Leino, A.-R.; Mäklin, J.; Halonen, N.; Shchukarev, A.; Konya, Z.; Jantunen, H.; Kordas, K. Room Temperature Hydrogen Sensors Based on Metal Decorated WO_3 Nanowires. *Sens. Actuators B* **2013**, *186*, 90−95.

(12) Boudiba, A.; Roussel, P.; Zhang, C.; Olivier, M.-G.; Snyders, R.; Debliquy, M. Sensing Mechanism of Hydrogen Sensors Based on Palladium-Loaded Tungsten Oxide (Pd−WO_3). *Sens. Actuators B* **2013**, *187*, 84−93.

(13) Gu, G.; Zheng, B.; Han, W. Q.; Roth, S.; Liu, J. Tungsten Oxide Nanowires on Tungsten Substrates. *Nano Lett.* **2002**, *2*, 849−851.

(14) Baek, Y.; Yong, K. Controlled Growth and Characterization of Tungsten Oxide Nanowires Using Thermal Evaporation of WO_3 Powder. *J. Phys. Chem. C* **2007**, *111*, 1213−1218.

(15) Lee, K.; Seo, W. S.; Park, J. T. Synthesis and Optical Properties of Colloidal Tungsten Oxide Nanorods. *J. Am. Chem. Soc.* **2003**, *125*, 3408−3409.

(16) Ahn, M.-W.; Park, K.-S.; Heo, J.-H.; Kim, D.-W.; Choi, K. J.; Park, J.-G. On-Chip Fabrication of ZnO-Nanowire Gas Sensor with High Gas Sensitivity. *Sens. Actuators B* **2009**, *138*, 168−173.

(17) Park, J.; Lim, D.; Choi, Y.; Kim, D.; Choi, K.; Park, J. Laterally Grown SnO_2 Nanowires and Their NO_2 Gas Sensing Characteristics. *7th IEEE Conf. Nanotechnol. (IEEE NANO)* **2007**, 1054−1057.

(18) Choi, Y.-J.; Hwang, I.-S.; Park, J.-G.; Choi, K. J.; Park, J.-H.; Lee, J.-H. Novel Fabrication of An SnO_2 Nanowire Gas Sensor with High Sensitivity. *Nanotechnology* **2008**, *19*, 095508.

(19) Sberveglieri, G.; Concina, I.; Comini, E.; Falasconi, M.; Ferroni, M.; Sberveglieri, V. Synthesis and Integration of Tin Oxide Nanowires into An Electronic Nose. *Vacuum* **2012**, *86*, 532−535.

(20) Park, J. Y.; Choi, S.-W.; Kim, S. S. Junction-Tuned SnO_2 Nanowires and Their Sensing Properties. *J. Phys. Chem. C* **2011**, *115*, 12774−12781.

(21) Thong, L. V.; Hoa, N. D.; Le, D. T. T.; Viet, D. T.; Tam, P. D.; Le, A.-T.; Hieu, N. V. On-Chip Fabrication of SnO_2 Nanowire Gas Sensor: The Effect of Growth Time on Sensor Performance. *Sens. Actuators B* **2010**, *146*, 361−367.

(22) Khoang, N. D.; Hong, H. S.; Trung, D. D.; Duy, N. V.; Hoa, N. D.; Thinh, D. D.; Hieu, N. V. On-Chip Growth of Wafer-Scale Planar-Type ZnO Nanorod Sensors for Effective Detection of CO Gas. *Sens. Actuators B* **2013**, *181*, 529−536.

(23) Hieu, N. V.; Vuong, H. V.; Duy, N. V.; Hoa, N. D. A Morphological Control of Tungsten Oxide Nanowires by Thermal Evaporation Method for Sub-ppm NO_2 Gas Sensor Application. *Sens. Actuators B* **2012**, *171−172*, 760−768.

(24) Tong, P. V.; Hoa, N. D.; Quang, V. V.; Duy, N. V.; Hieu, N. V. Diameter Controlled Synthesis of Tungsten Oxide Nanorod Bundles for Highly Sensitive NO_2 Gas Sensors. *Sens. Actuators B* **2013**, *183*, 372−380.

(25) Hieu, N. V.; Thuy, L. T. B.; Chien, N. D. Highly Sensitive Thin Film NH_3 Gas Sensor Operating at Room Temperature Based on SnO_2/MWCNTs Composite. *Sens. Actuators B* **2008**, *129*, 888−895.

(26) Liu, X.; Zhang, J.; Yang, T.; Guo, X.; Wu, S.; Wang, S. Synthesis of Pt Nanoparticles Functionalized WO_3 Nanorods and Their Gas Sensing Properties. *Sens. Actuators B* **2011**, *156*, 918−923.

(27) Qin, Y.; Shen, W.; Li, X.; Hu, M. Effect of Annealing on Microstructure and NO_2-Sensing Properties of Tungsten Oxide Nanowires Synthesized by Solvothermal Method. *Sens. Actuators B* **2011**, *155*, 646−652.

(28) Chen, C.-H.; Wang, S.-J.; Ko, R.-M.; Kuo, Y.-C.; Uang, K.-M.; Chen, T.-M.; Liou, B.-W.; Tsai, H.-Y. The Influence of Oxygen Content in the Sputtering Gas on the Self-Synthesis of Tungsten

Oxide Nanowires on Sputter-Deposited Tungsten Films. *Nanotechnology* **2006**, *17*, 217−223.
(29) Meng, D.; Shaalan, N. M.; Yamazaki, T.; Kikuta, T. Preparation of Tungsten Oxide Nanowires and Their Application to NO_2 Sensing. *Sens. Actuators B* **2012**, *169*, 113−120.
(30) Hong, K.; Xie, M.; Hu, R.; Wu, H. Diameter Control of Tungsten Oxide Nanowires as Grown by Thermal Evaporation. *Nanotechnology* **2008**, *19*, No. 085604.
(31) Hong, K.; Xie, M.; Hu, R.; Wu, H. Synthesizing Tungsten Oxide Nanowires by A Thermal Evaporation Method. *Appl. Phys. Lett.* **2007**, *90*, No. 173121.
(32) Zhang, H.; Xu, T. T.; Tang, M.; Her, T.; Li, S. Selective Growth of Tungsten Oxide Nanowires via A Vapor-Solid Process. *J. Vac. Sci. Technol. B Microelectron. Nanom. Struct.* **2010**, *28*, 310.
(33) Sysoev, V. V.; Schneider, T.; Goschnick, J.; Kiselev, I.; Habicht, W.; Hahn, H.; Strelcov, E.; Kolmakov, A. Percolating SnO_2 Nanowire Network as A Stable Gas Sensor: Direct Comparison of Long-Term Performance Versus SnO_2 Nanoparticle Films. *Sens. Actuators B* **2009**, *139*, 699−703.
(34) Chem, J. M.; Vuong, N. M.; Jung, H.; Kim, D.; Kim, H.; Hong, S. Realization of An Open Space Ensemble for Nanowires: A Strategy for the Maximum Response in Resistive Sensors. *J. Mater. Chem.* **2012**, *22*, 6716−6725.
(35) Qin, Y.; Li, X.; Wang, F.; Hu, M. Solvothermally Synthesized Tungsten Oxide Nanowires/Nanorods for NO_2 Gas Sensor Applications. *J. Alloys Compd.* **2011**, *509*, 8401−8406.
(36) Le, D. T. T.; Duy, N. V.; Tan, H. M.; Trung, D. D.; Trung, N. N.; Van, P. T. H.; Hoa, N. D.; Hieu, N. V. Density-Controllable Growth of SnO_2 Nanowire Junction-Bridging Across Electrode for Low-Temperature NO_2 Gas Detection. *J. Mater. Sci.* **2013**, *48*, 7253−7259.
(37) Law, J. B. K.; Boothroyd, C. B.; Thong, J. T. L. Site-Specific Growth of ZnO Nanowires from Patterned Zn via Compatible Semiconductor Processing. *J. Cryst. Growth* **2008**, *310*, 2485−2492.
(38) Ramgir, N. S.; Mulla, I. S.; Vijayamohanan, K. P. A Room Temperature Nitric Oxide Sensor Actualized from Ru-Doped SnO_2 Nanowires. *Sens. Actuators B* **2005**, *107*, 708−715.
(39) Teschner, D.; Farra, R.; Yao, L.; Schlögl, R.; Soerijanto, H.; Schomäcker, R.; Schmidt, T.; Szentmiklósi, L.; Amrute, A. P.; Mondelli, C.; Pérez-Ramírez, J.; Novell-Leruth, G.; López, N. An Integrated Approach to Deacon Chemistry on RuO_2-Based Catalysts. *J. Catal.* **2012**, *285*, 273−284.
(40) Qin, Y.; Sun, X.; Li, X.; Hu, M. Room Temperature NO_2-Sensing Properties of Ti-Added Nonstoichiometric Tungsten Oxide Nanowires. *Sens. Actuators B* **2012**, *162*, 244−250.
(41) Na, C. W.; Woo, H.-S.; Kim, I.-D.; Lee, J.-H. Selective Detection of NO_2 and C_2H_5OH Using A Co_3O_4-Decorated ZnO Nanowire Network Sensor. *Chem. Commun.* **2011**, *47*, 5148−5150.
(42) Shaalan, N. M.; Yamazaki, T.; Kikuta, T. NO_2 Response Enhancement and Anomalous Behavior of n-Type SnO_2 Nanowires Functionalized by Pd Nanodots. *Sens. Actuators B* **2012**, *166−167*, 671−677.
(43) Choi, S.-W.; Jung, S.-H.; Kim, S. S. Significant Enhancement of the NO_2 Sensing Capability in Networked SnO_2 Nanowires by Au Nanoparticles Synthesized Via γ-Ray Radiolysis. *J. Hazard. Mater.* **2011**, *193*, 243−248.
(44) Kim, S. S.; Park, J. Y.; Choi, S.-W.; Na, H. G.; Yang, J. C.; Kim, H. W. Enhanced NO_2 Sensing Characteristics of Pd-Functionalized Networked In_2O_3 Nanowires. *J. Alloys Compd.* **2011**, *509*, 9171−9177.
(45) Chueh, Y.-L.; Hsieh, C.-H.; Chang, M.-T.; Chou, L.-J.; Lao, C. S.; Song, J. H.; Gan, J.-Y.; Wang, Z. L. RuO_2 Nanowires and RuO_2/TiO_2 Core/Shell Nanowires: From Synthesis to Mechanical, Optical, Electrical, and Photoconductive Properties. *Adv. Mater.* **2007**, *19*, 143−149.
(46) Kolmakov, A.; Klenov, D. O.; Lilach, Y.; Stemmer, S.; Moskovits, M. Enhanced Gas Sensing by Individual SnO_2 Nanowires and Nanobelts Functionalized with Pd Catalyst Particles. *Nano Lett.* **2005**, *5*, 667−673.
(47) Park, S.; Kim, H.; Jin, C.; Choi, S.-W.; Kim, S. S.; Lee, C. Enhanced CO Gas Sensing Properties of Pt-Functionalized WO_3 Nanorods. *Thermochim. Acta* **2012**, *542*, 69−73.
(48) Epling, W. S.; Campbell, L. E.; Yezerets, A.; Currier, N. W.; Parks, J. E. Overview of the Fundamental Reactions and Degradation Mechanisms of NO_x Storage/Reduction Catalysts. *Catal. Rev.* **2004**, *46*, 163−245.
(49) Wang, H.; Schneider, W. F. Adsorption and Reactions of NO_x on RuO_2(110). *Catal. Today* **2011**, *165*, 49−55.